

Spin wave effects in transport between a ferromagnet and a Weyl semimetal surface

A. Kononov,¹ O.O. Shvetsov,^{1,2} A.V. Timonina,¹ N.N. Kolesnikov,¹ and E.V. Deviatov¹

¹*Institute of Solid State Physics of the Russian Academy of Sciences, Chernogolovka, Moscow District, 2 Academician Ossipyan str., 142432 Russia*

²*Moscow Institute of Physics and Technology, Institutskiy per. 9, Dolgoprudny, 141700 Russia*
(Dated: July 11, 2018)

We experimentally investigate spin-polarized transport between a ferromagnetic Ni electrode and a surface of Weyl semimetal, realized in a thick WTe₂ single crystal. For highly-transparent Ni-WTe₂ planar junctions, we observe non-Ohmic $dV/dI(I)$ behavior with an overall increase of differential resistance dV/dI with current bias, which is accomplished by current-induced switchings. This behavior is inconsistent with trivial interface scattering, but it is well known for spin-polarized transport with magnon emission. Thus, we interpret the experimental results in terms of spin wave excitation in spin textures in the WTe₂ topological surface states, which is supported by the obtained magnetic field and temperature $dV/dI(I)$ dependencies.

PACS numbers: 73.40.Qv 71.30.+h

A strong area of interest in condensed matter physics is topological materials [1–4], which combines many non-trivial effects, table top test ground for high-energy physics theories and huge potential for applications, for example in spintronics or quantum computing. Recently new classes of topological materials with gapless bulk spectra called Dirac and Weyl semimetals have been proposed [5]. Similarly to topological insulators, Weyl semimetals have topologically protected Fermi arc surface states, which are connecting projections of Weyl nodes on the surface Brillouin zone [5].

WTe₂ is one of the realizations of type-II Weyl semimetal [6], where energy spectrum is tilted in momentum-energy space [7]. WTe₂ demonstrates giant nonsaturating magnetoresistance [8, 9]. Now it is connected with complex spin textures in WTe₂ [10–12]. Spin- and angle- resolved photoemission spectroscopy (SARPES) data indeed demonstrate spin-polarized surface Fermi arcs, and spin polarized Fermi pockets in bulk spectrum [13, 14], see Fig. 1.

Intriguing spin properties of Weyl semimetals make it attractive material for spin investigations. Giant intrinsic Spin Hall Effect was recently predicted in TaAs based Weyl semimetals [15] while SARPES measurements demonstrated nearly full spin polarization of Fermi arcs in TaAs [16, 17]. Currently there are two main spin transport approaches: illumination with polarized light and spin injection from ferromagnetic contact [18]. In the latter case one can additionally expect back action of the semimetal on the ferromagnet in the form of spin-torque, which could lead even to remagnetization of ferromagnetic contact [19]. The generation of both out-of-plane and in-plane spin-torque has been demonstrated recently in few layers WTe₂ at room temperature with ST-FMR and second harmonic Hall measurements [20]. On the other hand, current-induced excitation of spin waves, or magnons, is possible at large electrical current densities for normal-ferromagnet junctions [21–24]. Thus, it is rea-

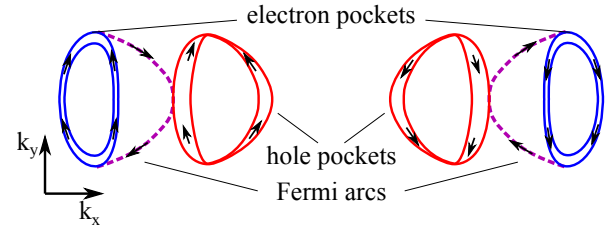


FIG. 1. (Color online) Sketch of Fermi arcs in (001) WTe₂ surface Brillouin zone, and spin polarized Fermi pockets in bulk WTe₂ spectrum [13, 14]. Arrows indicate spin projections, which are defined by the Weyl surface states dispersion due to spin-momentum locking [10–12].

sonable to study spin-polarized transport between a ferromagnet and a Weyl semimetal surface.

Here, we experimentally investigate spin-polarized transport between a ferromagnetic Ni electrode and a surface of Weyl semimetal, realized in a thick WTe₂ single crystal. For highly-transparent Ni-WTe₂ planar junctions, we observe non-Ohmic $dV/dI(I)$ behavior with an overall increase of differential resistance dV/dI with current bias, which is accomplished by current-induced switchings. This behavior is inconsistent with trivial interface scattering, but it is well known for spin-polarized transport with magnon emission. Thus, we interpret the experimental results in terms of spin wave excitation in spin textures in the WTe₂ topological surface states, which is supported by the obtained magnetic field and temperature $dV/dI(I)$ dependencies.

WTe₂ compound was synthesized from elements by reaction of metal with tellurium vapor in the sealed silica ampule. The WTe₂ crystals were grown by the two-stage iodine transport [25], that previously was successfully applied [25, 26] for growth of other metal chalcogenides like NbS₂ and CrNb₃S₆. The WTe₂ composition is verified by energy-dispersive X-ray spectroscopy. The X-ray diffraction (Oxford diffraction Gemini-A, MoK α)

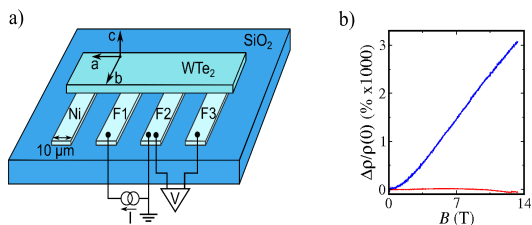


FIG. 2. (Color online) (a) Sketch of the sample with nickel contacts to the bottom surface of a WTe_2 crystal (not to the scale). 50 nm thick ferromagnetic nickel leads are formed on the insulating SiO_2 substrate. A WTe_2 single crystal is transferred on top of the leads with $\approx 10 \mu\text{m}$ overlap, forming planar Ni- WTe_2 junctions. Charge transport is investigated in a standard three-point technique: the studied contact (F2) is grounded and two other contacts (F1 and F3) are used for applying current and measuring WTe_2 potential. The main WTe_2 crystallographic directions are denoted by arrows. (b) Large positive magnetoresistance $\rho(B) - \rho(B = 0)/\rho(B = 0)$ for our WTe_2 samples at 1.2 K in normal magnetic field (the blue curve). It goes to zero in parallel one (the red curve), as it has been shown for WTe_2 Weyl semimetal [8]. The current is parallel to the a axis of WTe_2 .

confirms $Pmn2_1$ orthorhombic single crystal WTe_2 with lattice parameters $a = 3.4875 \text{ \AA}$, $b = 6.2672 \text{ \AA}$, and $c = 14.0630 \text{ \AA}$.

A sample sketch is presented in Fig. 2 (a). 50 nm thick nickel film is thermally evaporated on the insulating SiO_2 substrate mounted on the in-plane magnetized sample holder. $10 \mu\text{m}$ wide ferromagnetic leads are formed by photolithography and lift-off technique. The WTe_2 crystal (with dimensions $500 \mu\text{m} \times 100 \mu\text{m} \times 0.5 \mu\text{m}$) is transferred on top of the leads with $\approx 10 \times 10 \mu\text{m}^2$ overlap and weakly pressed to form planar Ni- WTe_2 junctions.

We investigate transport properties of single Ni- WTe_2 junction by a three-point technique, see Fig. 2 (a): a studied contact F2 is grounded, two other contacts F1 and F3 are employed to apply current and measure voltage respectively. To obtain $dV/dI(I)$ characteristics we sweep dc-current modulated by low (below $2 \mu\text{A}$, $f = 2 \text{ kHz}$) ac current. We measure dc and ac voltage simultaneously using voltmeter and lock-in amplifier correspondingly. Measured ac signal is independent of frequency in 1-5 kHz range, which is defined by applied ac filters.

In a three-point technique, the measured potential V reflects in-series connected resistances of the Ni- WTe_2 junction, some part of the WTe_2 crystal, and the Ni lead with the grounding wire. To exclude the latter term, additional connection to the grounded F2 lead is used, as depicted in Fig. 2. From $dV/dI(I)$ independence on the particular choice of current and voltage probes to the WTe_2 crystal, we verify that the Ni- WTe_2 junction resistance dominates in the obtained $dV/dI(I)$ curves.

We check by standard magnetoresistance measurements that our WTe_2 samples demonstrate large, non-

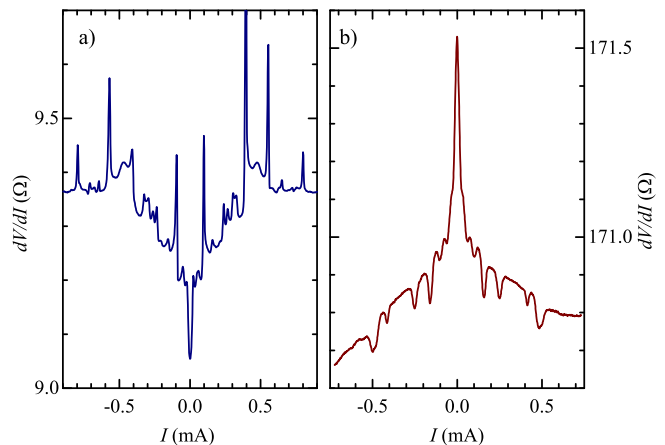


FIG. 3. (Color online) Typical examples of non-Ohmic $dV/dI(I)$ behavior for the two limiting cases of Ni- WTe_2 junction resistance: (a) for transparent Ni- WTe_2 interface, dV/dI is unexpectedly rising at low biases with saturation at higher ones; (b) for resistive junctions, dV/dI is diminishing with bias, which is usual tunnel behavior. In both cases, current-induced switching of dV/dI can be seen as sharp dV/dI peaks or dips, which are symmetric with respect to the bias sign. These features are well reproducible in different cooling cycles. The curves are obtained at 30 mK in zero magnetic field.

saturation positive magnetoresistance $\rho(B) - \rho(B = 0)/\rho(B = 0)$ in normal magnetic field, which goes to zero in parallel one, see Fig. 2 (b), as it has been shown for WTe_2 Weyl semimetal [8]. To extract features specific to WTe_2 Weyl semimetal surface states, the measurements are performed in a dilution refrigerator at temperatures from 30 mK to 1.2 K with different orientations of the magnetic field to the junction plane.

Despite of equally prepared Ni- WTe_2 junctions, there are serious device-to-device fluctuations of the junction resistance. Fig. 3 provides typical examples of low-temperature $dV/dI(I)$ characteristics for the two limiting cases.

For the transparent interface with low Ni- WTe_2 junction resistance, dV/dI is rising at low biases with saturation at higher ones, see Fig. 3 (a). This behavior is inconsistent with trivial impurity or roughness scattering at the interface, which can generally be described as tunneling through a potential barrier. On the other hand, an overall symmetric increase in dV/dI is a familiar effect for electron scattering by emission of phonons and magnons [27].

In contrast, $dV/dI(I)$ demonstrates clear tunnel behavior for low-transparency junctions, see Fig. 3 (b): $dV/dI(I)$ is slightly asymmetric, the differential resistance dV/dI is diminishing with bias.

For both realizations of Ni- WTe_2 junctions, we observe current-induced switchings of dV/dI at high currents. They appear as sharp dV/dI peaks or dips in Fig. 3 (a) and (b), respectively. These dV/dI features

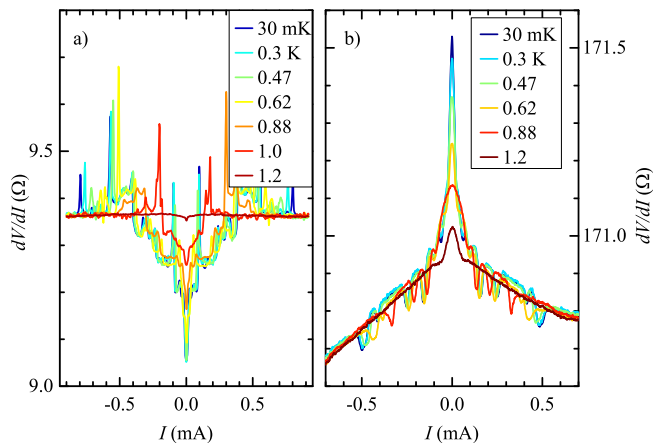


FIG. 4. (Color online) Temperature evolution of $dV/dI(I)$ characteristics for high- (a) and low- (b) transparency Ni-WTe₂ junctions. The effect of temperature is weak below 0.5 K. At higher temperatures, dV/dI dips and peaks amplitudes and overall $dV/dI(I)$ non-linearity are diminishing, until their complete disappearance above 1 K. The curves are obtained in zero magnetic field.

are well reproducible in different cooling cycles. They are symmetric with respect to the current sign. There is no noticeable hysteresis with the current sweep direction for experimental $dV/dI(I)$ curves.

The observed $dV/dI(I)$ non-linearity as well as current-induced dV/dI switchings are sensitive to the magnetic field and temperature.

Fig. 4 shows temperature evolution of $dV/dI(I)$ characteristics for high- and low-transparency junctions, see (a) and (b) panels, respectively. The effect of temperature is weak below 0.5 K. At higher temperatures, $dV/dI(I)$ non-linearity is diminishing. Above 1 K, the differential resistance is almost constant in Fig. 4 (a), so $dV/dI(I)$ s are of standard Ohmic behavior. In contrast, $dV/dI(I)$ is still non-linear for the resistive junction in Fig. 4 (b), while dV/dI dips are also suppressed above 1 K.

Fig. 5 demonstrates evolution of $dV/dI(I)$ curves with magnetic field, which is applied along a, b and c WTe₂ crystal axes, respectively. The effect of magnetic field is sophisticated: in high fields, the zero-bias nonlinearity is suppressed, while the level of $dV/dI(I)$ high-current saturation is unchanged, so that $dV/dI(I)$ curve is of clear Ohmic behavior above some magnetic field. This field is smaller for normal field orientation, see Fig. 5 (c), while there is no difference for two in-plane orientations, cp. Fig. 5 (a) and (b). In lower fields, the positions of dV/dI current-induced switchings are shifting to smaller currents. The effect of magnetic field on the low-transparent junction is similar to the presented in Fig. 5. The gradual evolution of switchings' positions also proves excellent reproducibility of these dV/dI features in addition to their stability in thermal cycling.

We should connect the obtained results with spin-dependent transport between a ferromagnetic Ni lead and WTe₂ surface states:

(i) A ferromagnetic lead is essential, since neither current-induced dV/dI switchings nor an overall symmetric increase in dV/dI can be observed for normal or superconducting leads to a single WTe₂ crystal for different junction transparencies [28, 29].

(ii) Both current-induced dV/dI switchings and overall $dV/dI(I)$ behavior can be controlled by magnetic field, see Fig. 5.

(iii) Strong temperature dependence in the 30 mK-1.2 K range can only originate from WTe₂ surface state, since transport properties of Ni layer and well compensated WTe₂ bulk carriers [9] are invariant in this temperature range.

Spin effects can be anticipated in WTe₂ surface states due to the presence of spin textures in the WTe₂ Fermi arcs [10, 11, 13, 14], see Fig. 1. In principle, a junction between a ferromagnetic Ni layer and a WTe₂ surface can be regarded as a spin valve device. The spin valves are the sandwich structures, where spin-dependent scattering affects the magnetic moments of the spin-polarized layers, while their mutual orientation defines the differential resistance [27]. dV/dI switchings have been reported for spin valves [27], but they are necessarily asymmetric with respect to the bias sign, and also accomplished by well-defined hysteresis [27], which is obviously not the case in Figs. 3 and 5.

Inelastic transport with magnon emission [24] is a more realistic variant, since the switchings are governed [22] by magnetic field in Fig. 5.

Let us start from the low-transparent junction in Figs. 3 (b) and 4 (b). Trivial tunneling is the main effect, which results in a standard non-linear $dV/dI(I)$ curve with dV/dI diminishing with bias increase. In tunneling events, hot electrons appear above the Fermi level. They thermalize by scattering with lattice defects, phonons, or other electrons. This process is accomplished by spin polarization of the ferromagnetic lead and spin textures in the WTe₂ surface state. In this case, hot electrons should additionally rotate their spins to be absorbed. Conservation of total spin results in excitation of a magnon, which opens an additional inelastic channel. Thus, the current is enhanced, which is observed as sharp dips in differential resistance dV/dI , as it has also been previously reported for the vacuum-separated metallic contacts [24].

Spin-wave effects are even clearer for highly-transparent junctions, see Fig. 3 (a), because of negligible interface barrier. For example, the current-induced switchings can not be connected with the potentially inhomogeneous interface in this case.

The crucial point is that the low-temperature zero-bias resistance is smaller than the value, obtained at high bi-

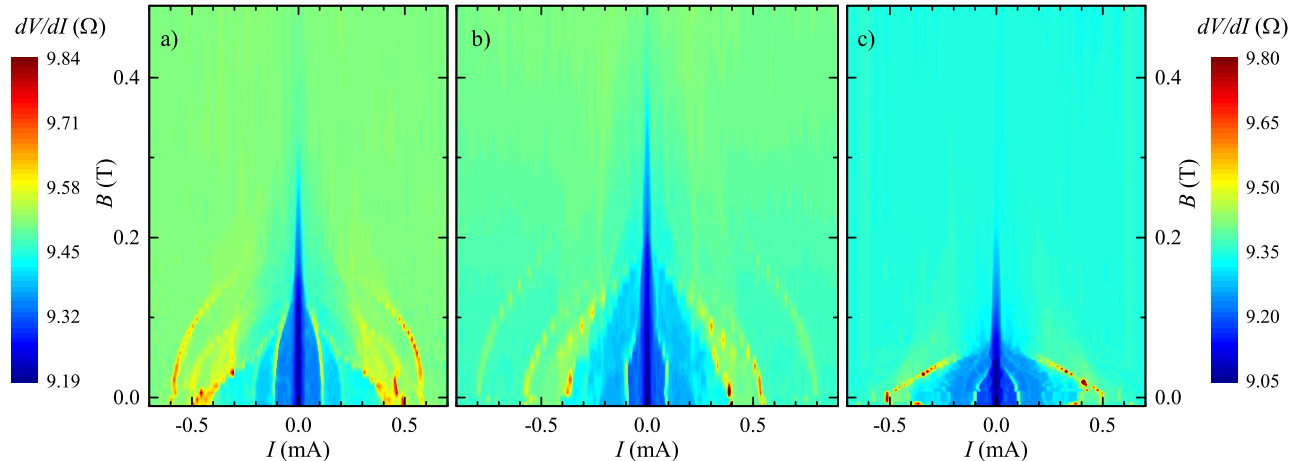


FIG. 5. (Color online) Evolution of $dV/dI(I)$ curves with magnetic field, which is applied along a, b and c WTe_2 crystal axes, respectively. Qualitative effect is similar: the level of $dV/dI(I)$ high-current saturation is constant; the zero-bias nonlinearity is suppressed; the positions of dV/dI current-induced switchings are shifting to smaller currents. The effect is stronger in normal field, while there is no difference for two in-plane orientations. Color scale on the left reflects differential resistance levels in (a), color scale on the right refers to (b) and (c). The curves are obtained at 30 mK for the transparent Ni- WTe_2 junction from Fig. 3 (a). The gradual evolution of switchings' positions also proves excellent reproducibility of these dV/dI features.

ases, temperatures, or magnetic fields, see Figs. 3 (a), 4 (a), and 5. At zero bias, one can expect that spin polarization of some carriers at the WTe_2 surface is aligned parallel to one in the ferromagnet due to the complicated spin texture of the topological Fermi arc surface state, see Fig. 1. This allows a direct transport channel even for spin-polarized carriers, which is reflected in low junction resistance at zero bias. When increasing the current through the surface state, spin-momentum locking [10, 11, 13, 14] produces preferable spin polarization. It suppresses transport due to the requirement on spin rotation in transport events, which is reflected as the overall dV/dI increase for both signs of the current. This picture is consistent with the magnetic-field and temperature dependences of $dV/dI(I)$: spin alignment at zero bias disappears when high magnetic field or temperature destroys spin textures of the topological surface state, so the zero-bias differential resistance is at the normal (saturated) value, see Figs. 4 and 5.

Similarly to the transparent metallic junctions [21, 22], the onset of the current-driven magnon excitations appears as dV/dI peaks in Fig. 3. In low magnetic fields, the peaks positions are shifted [22] to lower currents, see Fig. 5, because an external field simplifies spin-wave excitation in the WTe_2 surface state. We wish to emphasize, that the magnon excitation occurs in the WTe_2 surface state, since transport properties of Ni layer and well compensated WTe_2 bulk carriers [9] are invariant below 1 K. Thus, our results can be regarded as direct manifestation of spin textures in WTe_2 surface states in transport experiment.

As a conclusion, we experimentally investigate spin-polarized transport between a ferromagnetic Ni electrode and a surface of Weyl semimetal, realized in a thick WTe_2 single crystal. For highly-transparent Ni- WTe_2 planar junctions, we observe non-Ohmic $dV/dI(I)$ behavior with an overall increase of differential resistance dV/dI with current bias, which is accomplished by current-induced switchings. This behavior is inconsistent with trivial interface scattering, but it is well known for spin-polarized transport with magnon emission. Thus, we interpret the experimental results in terms of spin wave excitation in spin textures in the WTe_2 topological surface states, which is supported by the obtained magnetic field and temperature $dV/dI(I)$ dependencies.

We wish to thank V.T. Dolgoplov and S.A. Tarasenko for fruitful discussions, and S.S. Khasanov for X-ray sample characterization. We gratefully acknowledge financial support by the RFBR (project No. 16-02-00405) and RAS.

-
- [1] M. Z. Hasan and C. L. Kane, Rev. Mod. Phys. 82, 3045 (2010).
 - [2] X.-L. Qi and S.-C. Zhang, Rev. Mod. Phys. 83, 1057 (2011).
 - [3] A. Bansil, H. Lin, and T. Das, Rev. Mod. Phys. 88, 021004 (2016).
 - [4] C.-K. Chiu, J. C. Teo, A. P. Schnyder, and S. Ryu, Rev. Mod. Phys. 88, 035005 (2016).
 - [5] As a recent review see N.P. Armitage, E.J. Mele, and A. Vishwanath, Rev. Mod. Phys. 90, 015001 (2018).

- [6] P. Li, Y. Wen, X. He, Q. Zhang, C. Xia, Z.-M. Yu, S.A. Yang, Z. Zhu, H.N. Alshareef, X.-X. Zhang, *Nature Comm.* **8**, 2150 (2017)
- [7] A.A. Soluyanov, D. Gresch, Z. Wang, Q. Wu, M. Troyer, X. Dai, B.A. Bernevig, *Nature* **527**, 495 (2015).
- [8] M.N. Ali, J. Xiong, S. Flynn, J. Tao, Q.D. Gibson, L.M. Schoop, T. Liang, N. Haldolaarachchige, M. Hirschberger, N.P. Ong, and R.J. Cava, *Nature (London)* **514**, 205 (2014).
- [9] H.Y. Lv, W.J. Lu, D.F. Shao, Y. Liu, S.G. Tan, and Y.P. Sun, *Europhys. Lett.* **110**, 37004 (2015).
- [10] J. Jiang, F. Tang, X.C. Pan, H.M. Liu, X.H. Niu, Y.X. Wang, D.F. Xu, H.F. Yang, B.P. Xie, F.Q. Song, P. Dudin, T.K. Kim, M. Hoesch, P.K. Das, I. Vobornik, X.G. Wan, and D.L. Feng, *Phys. Rev. Lett.* **115**, 166601 (2015).
- [11] D. Rhodes, S. Das, Q.R. Zhang, B. Zeng, N.R. Pradhan, N. Kikugawa, E. Manousakis, and L. Balicas, *Phys. Rev. B* **92**, 125152 (2015).
- [12] Y. Wang, K. Wang, J. Reutt-Robey, J. Paglione, and M. S. Fuhrer, *Phys. Rev. B* **93**, 121108 (2016).
- [13] P.K. Das, D.D. Sante, I. Vobornik, J. Fujii, T. Okuda, E. Bruyer, A. Gyenis, B.E. Feldman, J. Tao, R. Ciancio, G. Rossi, M.N. Ali, S. Picozzi, A. Yadzani, G. Panaccione, and R.J. Cava, *Nature Comm.* **7**, 10847 (2016).
- [14] B. Feng, Y.-H. Chan, Y. Feng, R.-Y. Liu, M.-Y. Chou, K. Kuroda, K. Yaji, A. Harasawa, P. Moras, A. Barinov, W. Malaeb, C. Bareille, T. Kondo, S. Shin, F. Komori, T.-C. Chiang, Y. Shi, and I. Matsuda, *Phys Rev B* **94**, 195134 (2016).
- [15] Y. Sun, Y. Zhang, C. Felser, B. Yan, *Phys. Rev. Lett.* **117**, 146403 (2016).
- [16] B.Q. Lv, S. Muff, T. Qian, Z.D. Song, S.M. Nie, N. Xu, P. Richard, C.E. Matt, N.C. Plumb, L.X. Zhao, G.F. Chen, Z. Fang, X. Dai, J.H. Dil, J. Mesot, M. Shi, H.M. Weng, and H. Ding, *Phys. Rev. Lett.* **115**, 217601 (2015).
- [17] S.-Y. Xu, I. Belopolski, D.S. Sanchez, M. Neupane, G. Chang, K. Yaji, Z. Yuan, C. Zhang, K. Kuroda, G. Bian, C. Guo, H. Lu, T.-R. Chang, N. Alidoust, H. Zheng, C.-C. Lee, S.-M. Huang, C.-H. Hsu, H.-T. Jeng, A. Bansil, T. Neupert, F. Komori, T. Kondo, S. Shin, H. Lin, S. Jia, and M.Z. Hasan, *Phys. Rev. Lett.* **116**, 096801 (2016).
- [18] Y. Tserkovnyak, A. Brataas, G.E.W. Bauer, and B.I. Halperin, *Rev. Mod. Phys.* **77**, 1375 (2005).
- [19] J.C. Slonczewski, *J. Magn. Magn. Mater.* **159**, L1-L7 (1996).
- [20] D. MacNeill, G.M. Stiehl, M.H.D. Guimarães, R.A. Buhrman, J. Park and D.C. Ralph, *Nature Physics* **13**, 300 (2017).
- [21] M. Tsoi, A. G. M. Jansen, J. Bass, W.-C. Chiang, M. Seck, V. Tsoi, and P. Wyder, *Phys. Rev. Lett.*, **80**, 4281 (1998).
- [22] M. Tsoi, A. G. M. Jansen, J. Bass, W.-C. Chiang, V. Tsoi and P. Wyder, *Nature*, **406**, 46, (2000).
- [23] O. P. Balkashin, V. V. Fisun, I. K. Yanson, L. Yu. Triputen, A. Konovalenko, and V. Korenivski, *Phys. Rev. B*, **79**, 092419 (2009)
- [24] T. Balashov, A. F. Takács, I. M. Däne, A. Ernst, P. Bruno, and W. Wulfhekel, *Phys. Rev. B*, **78**, 174404 (2008)
- [25] E. B. Borisenko, V. A. Berezin, N. N. Kolesnikov, V. K. Gartman, D. V. Matveev, O. F. Shakhlevich, *Physics of the Solid State*, **59**, 1310, (2017).
- [26] A. Sidorov, A.E. Petrova, A.N. Pinyagin, N.N. Kolesnikov, S.S. Khasanov, S.M. Stishov, *JETP*, **122**, 1047, (2016).
- [27] E.B. Myers, D.C. Ralph, J.A. Katine, R.N. Louie, R.A. Buhrman, *Science*, **285**, 867 (1999).
- [28] O. O. Shvetsov, A. Kononov, A. V. Timonina, N. N. Kolesnikov, E. V. Deviatov, *JETP Letters*, (2018) <https://doi.org/10.1134/S0021364018120020>
- [29] A. Kononov, O. O. Shvetsov, S. V. Egorov, A. V. Timonina, N. N. Kolesnikov and E. V. Deviatov *EPL*, **122**, 27004 (2018) doi: 10.1209/0295-5075/122/27004